JOURNAL OF SOLID STATE CHEMISTRY 113, 420–433 (1994)

Relation between Electron Band Structure and Magnetic Bistability of Conduction Electrons in β-Ga_2O_3

L. Binet and D. Gourier[1]

Laboratoire de Chimie Appliquée de l'Etat Solide, URA 1466 CNRS, Ecole Nationale Supérieure de Chimie de Paris, 11 rue Pierre et Marie Curie, F-75231 Paris Cedex 05, France

and

C. Minot

Laboratoire de Chimie Organique Théorique, URA 506 CNRS, Université Pierre et Marie Curie, Boite 53, Bat. F 642, 4 place Jussieu, F-75252 Paris Cedex 05, France

Received November 29, 1993; in revised form March 16, 1994; accepted March 17, 1994

When slightly oxygen-deficient, β-Ga_2O_3 is an *n*-type semiconductor with conduction electrons exhibiting a bistable spin resonance. In this paper, we discuss the relation between the electronic structure of gallium oxide and this peculiar magnetic property. The electron band structure of β-Ga_2O_3 is computed with the extended Hückel method. The calculations show that the conduction band has a strong 4*s* gallium character ($\approx$ 60%), with a quasi-exclusive contribution of the octahedral gallium ions to the band edge. The conduction band also exhibits a quasi-one-dimensional character with bandwidths much larger along the b* axis than along the a* or c* axes. Therefore, conduction electrons are essentially delocalized along the octahedral chains of the structure, whereas the surrounding tetrahedral chains are not occupied. The low-dimensional character of the electronic structure of β-Ga_2O_3 is confirmed by ESR and ENDOR spectroscopies of Ti^{3+} ions in substitutional octahedral sites, which provide evidence for predominant Ti–Ga superhyperfine interactions extending as far as the second neighboring Ga in the chain direction. It is also shown that the two conditions necessary for the existence of bistable conduction electron spin resonance, i.e., a strong dynamic nuclear polarization and a narrow ESR line, can be quantitatively accounted for by the important 4*s* gallium character of the conduction band and by its pronounced anisotropy. © 1994 Academic Press, Inc.

1. INTRODUCTION

Gallium β-Ga_2O_3 oxide is normally an insulator, with a forbidden energy gap of 4.84 eV. However, it is generally an *n*-type semiconductor due to oxygen vacancies individually compensated by two electrons, forming shallow donors with ionization energy $E_d \approx 0.03$–0.04 eV (1). Conduction electrons in solids can often be detected by electron spin resonance, and give invariably a more or less broad single line as the result of the motional narrowing of the spin–spin interactions (2). The conduction electron spin resonance (CESR) line of semiconducting gallium oxide crystals exhibits several interesting features: (i) its width ΔB is very small, slightly sample-dependent, with a mean value of about 0.05 mT at room temperature and at low microwave power (3); (ii) the saturation of the CESR line produces a strong dynamic nuclear polarization of gallium nuclei, resulting in a nuclear magnetic field B_n which adds to the external magnetic field B_0. This is the so-called Overhauser effect (4), which produces a shift of the CESR line toward low field by an amount equal to B_n. The Overhauser shift has been recently studied in β-Ga_2O_3 and was found to be surprisingly strong, about 0.4 mT at 150 K and 0.2 mT even at room temperature (5). The observation of this phenomenon at room temperature is, to our knowledge, unexpected for an inorganic semiconductor, but it has recently been studied in several one-dimensional organic conductors (6). In the latter case, however, the Overhauser shifts are almost three orders of magnitude less than those for β-Ga_2O_3. The most interesting feature of the CESR of β-Ga_2O_3 is that it is bistable, which means that the CESR line exhibits hysteresis upon sweeping up and down the external magnetic field B_0 (3). Hysteresis of the CESR intensity was also observed upon increasing and decreasing variations of the microwave power (5). It has been demonstrated (7) that this bistability is a consequence of both the small CESR linewidth and the strength of the Overhauser effect. Lineshapes of bistable CESR signals were successfully simulated with a model of noninteracting free electrons in the conduction band of β-Ga_2O_3 (5), indicating that bistability and hysteresis can exist at the level of isolated electrons.

[1] To whom correspondence should be addressed.

0022-4596/94 $6.00
Copyright © 1994 by Academic Press, Inc.
All rights of reproduction in any form reserved.

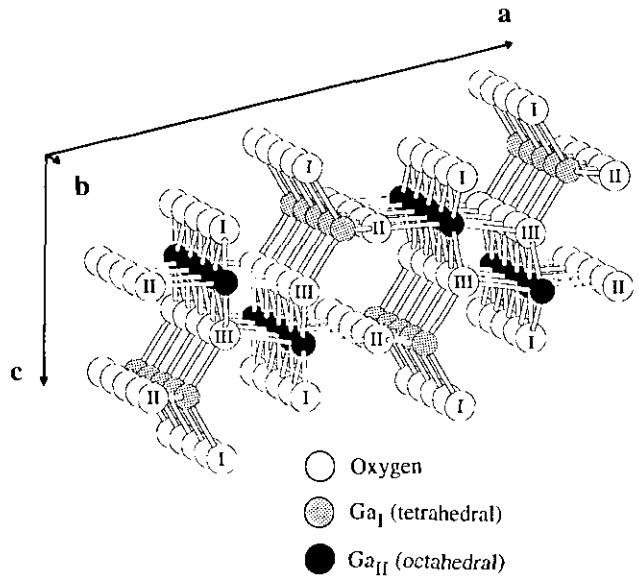

FIG. 1. Structure of β-Ga_2O_3.

Bistable conduction electron spin resonance (which will hereafter be referred to as BCESR) can be observed in β-Ga_2O_3 even at room temperature (5), and it does not seem to have been reported earlier for other conducting materials, except for an isolated observation in small metallic lithium particles at 4 K (8). Owing to the ease of observation of this phenomenon with a standard ESR spectrometer, it can be anticipated that BCESR is probably not a general property of semiconductors and metals, and its sole observation in β-Ga_2O_3 should be related to a peculiar feature of the electronic structure of this compound. We deduced from the equation governing the bistable hysteresis that conduction electrons of a conducting material may possess this property if they move in a conduction band with an important contribution from *s* orbitals of the element containing the nuclear spin, and if the CESR line is very narrow (7). In semiconductors and metals, the latter condition is generally fulfilled when the dimensionality of the material is low, since the narrowest ESR lines are found for 1D organic (6) and organometallic conductors (9, 10).

However, from the mere structural standpoint, β-Ga_2O_3 cannot be considered to be a low-dimensional material. It is monoclinic with space group $C2/m$ and with lattice parameters **a** = 12.23 Å, **b** = 3.04 Å, **c** = 5.80 Å, and β = 103.7° (11). The lattice is composed of two types of gallium ions, hereafter referred to as Ga_I and Ga_{II}, located respectively in tetrahedral and octahedral coordination sites (Fig. 1), and three kinds of oxygen ions, referred to as O_I, O_{II}, and O_{III}. Oxygens O_I and O_{II} lie respectively in and out of the symmetry plane. They are both in a threefold coordination while O_{III} is in tetrahedral coordination. The β-Ga_2O_3 structure is made up of double chains of edge-sharing octahedra runing along the **b** axis. These chains are linked to single chains of tetrahedra along **b** in such a way that each double octahedral chain is surrounded by six tetrahedral chains. Despite this linear arrangement along **b**, low dimensionality is not obvious if we consider gallium–gallium distances. As can be seen from Table 1, distances from a gallium ion Ga_I or Ga_{II} to its first six neighbors vary within a very small range, 3.04 to 3.61 Å. Therefore a given gallium is surrounded by many closely spaced neighbors either in octahedral or in tetrahedral sites, so that we would not expect low-dimensional interactions on the sole basis of structural considerations.

Since CESR bistability is possible only for strong Overhauser shifts and very narrow CESR linewidths, which are both conditioned by the orbital composition and the anisotropy of the conduction band, it is of primary interest for a deeper understanding of magnetic bistability of conduction electrons in β-Ga_2O_3 to determine the gross features of its band structure. In Section III, we describe the electronic structure of β-Ga_2O_3 calculated in the crystalline extension of the extended Hückel method (12), where it becomes evident that the conduction band exhibits a strong 1D character and conduction electrons move along chains principally made of 4*s* orbitals of gallium ions in octahedral coordination. Direct evidence of low-dimensional electron structure of a conducting material is usually provided by the study of the transport properties, such as conductivity and Hall effect. Despite the fact that several works have already been devoted to conductivity and Hall measurements on β-Ga_2O_3 (1, 13), the anisotropy of the electronic conductivity has not yet been studied. Moreover, to our knowledge, only one paper gives data on conductivity at low temperatures (1). Pulsed ESR spectroscopy is also well adapted to determine the anisotropy of electronic conductivity (6, 14). However, to our knowledge, such experiments on β-Ga_2O_3 have not been performed so far.

TABLE 1
Distances (in Å) from a Gallium Ga_I or Ga_{II} to the First Six Neighbors

	Site			
ith Neighbor	Ga_I		Ga_{II}	
1	Ga_I (2)	3.04	Ga_{II} (2)	3.04
2	Ga_{II}	3.28	Ga_{II} (2)	3.11
3	Ga_{II} (2)	3.30	Ga_I	3.28
4	Ga_{II} (2)	3.33	Ga_I (2)	3.30
5	Ga_{II} (2)	3.45	Ga_I (2)	3.33
6	Ga_I	3.61	Ga_I (2)	3.45

A simple and direct method to identify anisotropic electronic interactions is to measure the superhyperfine (shf) interaction between a paramagnetic impurity as for example a transition metal element and the nearest neighbor nuclei. Particularly, the parameter of interest is the Fermi contact term of the shf interaction, which is directly related to covalency parameters (15). If this interaction is too small to be observed on the ESR spectrum, a considerable resolution enhancement is achieved by using electron nuclear double resonance (ENDOR) spectroscopy (16). Since the first elements of the $3d$ transition metals have the smallest contraction of d orbitals in the series, they are more sensitive to orbital interactions with their neighbors. In Section IV, we use Ti^{3+} as a paramagnetic probe to study the anisotropy of cation–cation interactions. Surprisingly, it is found that titanium–gallium interactions along **b** are so strong that they are directly observed on the ESR spectrum of Ti^{3+}. We show, by combining ESR and a preliminary ENDOR study of ^{69}Ga and ^{71}Ga nuclei, that there is a significant Fermi contact interaction up to the second neighbor gallium ions along the **b** direction. This interaction is larger than the interaction with the first neighbor along other directions. The evidence of 1D cation–cation interactions in β-Ga_2O_3 having been demonstrated in Section IV, we finally discuss in Section V the relations between the structure of the conduction band and the magnetic parameters at the origin of the BCESR phenomenon in this compound.

II. EXPERIMENTAL

Crystal Growth

Single crystals of β-Ga_2O_3 : Ti were gown by the floating zone method in an image furnace (17) or by the Verneuil method (18) under slightly reducing conditions ($H_2/O_2 = 2.2$). The starting Ga_2O_3 powder, purchased from Rhône–Poulenc, was 99.99% pure and was mixed with a TiO_2 powder in such proportions that Ti/Ga ≈ 0.2%. The following mechanism for the insertion of Ti^{4+} into β-Ga_2O_3 can be proposed. It is similar to the one suggested by Harwig *et al.* (13c) for the insertion of Zr^{4+}:

$$3TiO_2 \rightarrow 3Ti_{Ga}^{\cdot} + V_{Ga}''' + 6O_O^x \qquad [1]$$

$$2TiO_2 \rightarrow 2Ti_{Ga}^{\cdot} + O_i'' + 3O_O^x. \qquad [2]$$

This mechanism assumes a substitutional position for Ti^{4+}, which will be justified in Section IV. Ti^{4+} ions are deep levels, which can trap the electrons released by the formation of oxygen vacancies,

$$O_O^x \rightarrow V_O^{\cdot\cdot} + 2e^- + 1/2O_2 \qquad [3]$$

$$Ti^{4+} + e^- \rightarrow Ti^{3+}, \qquad [4]$$

leading to Ti^{3+} ions. A ratio Ti/Ga ≈ 0.2% corresponds to $[Ti] \approx 8 \times 10^{19}$ cm^{-3}. As electron concentration does not exceed 10^{18}–10^{19} cm^{-3}, all the electrons are trapped on Ti^{4+} ions. This explains why no CESR signal is observed, but only a broad ESR line corresponding to spins localized in the vicinity of Ti ions.

ESR and ENDOR Measurements

ESR spectra were recorded at 110 K under nitrogen flow on an X-band 220D Bruker spectrometer equipped with a TE_{102} cavity. ENDOR spectra were recorded at 20 K with an Oxford Instruments ESR 9 continuous flow helium cryostat, a Bruker cavity working in the TM_{110} mode, and a 100 W ENI broadband power amplifier. ENDOR spectra were detected using frequency modulation at 12.5 kHz of the rf carrier. In the following, the NMR frequencies and the nuclear g-factors will be noted respectively ν_{n71}, g_{n71} for ^{71}Ga and ν_{n69}, g_{n69} for ^{69}Ga.

Band Structure Calculations

The band structure of β-Ga_2O_3 was computed in the crystalline extension of the extended Hückel method. For each Slater-type atomic orbital (AO) ϕ_μ, a corresponding Bloch sum $b_\mu(\mathbf{k})$ is built as follows:

$$b_\mu(\mathbf{k}) = \frac{1}{\sqrt{N}} \sum_{p=1}^{N} e^{i\mathbf{k}\cdot\mathbf{R}_p} \phi_\mu(\mathbf{r} - \mathbf{R}_p). \qquad [5]$$

Here the sum is made over the N cells in the solid and $\mathbf{k}$ is the wave vector of the Bloch state. The crystal orbitals $\psi_i(\mathbf{k})$ are expanded as linear combinations of the basis Bloch sums,

$$\psi_i(\mathbf{k}) = \sum_{\mu=1}^{n} c_{i\mu}(\mathbf{k}) b_\mu(\mathbf{k}), \qquad [6]$$

where n is the number of Bloch functions (i.e., the number of AOs in the cell) in the basis set. The Eigen energies $e_i(\mathbf{k})$ and the unknown coefficients $c_{i\mu}(\mathbf{k})$ are given by the solutions of the secular equations:

$$\det[\mathbf{H}(\mathbf{k}) - \mathbf{S}(\mathbf{k}) e_i(\mathbf{k})] = 0 \qquad [7]$$

$$(\mathbf{H}(\mathbf{k}) - \mathbf{S}(\mathbf{k}) e_i(\mathbf{k}))\mathbf{C} = 0 \quad \text{for } i = 1 \text{ to } n. \qquad [8]$$

here $\mathbf{C}$ is a vector, the components of which are the $c_{i\mu}(\mathbf{k})$'s. $\mathbf{S}(\mathbf{k})$ is the overlap matrix, and $\mathbf{H}(\mathbf{k})$ is the hamiltonian matrix. Their respective elements are defined by

$$S_{\mu\nu}(\mathbf{k}) = \langle b_\mu(\mathbf{k}) \,|\, b_\nu(\mathbf{k}) \rangle \qquad [9]$$

$$H_{\mu\nu}(\mathbf{k}) = \langle b_\mu(\mathbf{k}) \,|\, \mathbf{H}^{\text{eff}} \,|\, b_\nu(\mathbf{k}) \rangle. \qquad [10]$$

TABLE 2
Parameters Used in Extended Hückel Calculations

		$H^{eff}_{\mu\mu}$ (eV)	ζ
Ga^{3+}	4*p*	−6	2.20
	4*s*	−15	2.59
O^{2-}	2*p*	−14.8	2.275
	2*s*	−32.3	2.275

Note. $H^{eff}_{\mu\mu}$ and ζ are respectively the diagonal elements of the effective hamiltonian, and the Slater exponents.

The expansion of $S_{\mu\nu}(\mathbf{k})$ contains overlap integrals $\langle\phi_\mu(\mathbf{r}-\mathbf{R}_p)\,|\,\phi_\nu(\mathbf{r}-\mathbf{R}_q)\rangle$ which were in practice neglected when $|\mathbf{R}_p-\mathbf{R}_q|>8$ Å. Similarly, the $H_{\mu\nu}(\mathbf{k})$ expand on the $\langle\phi_\mu\,|\,\mathbf{H}^{eff}\,|\,\phi_\nu\rangle$ terms. The parameters in these calculations are the Slater exponents ζ of the Slater orbitals and the diagonal elements of the effective hamiltonian $\mathbf{H}^{eff}$, $\langle\phi_\mu\,|\,\mathbf{H}^{eff}\,|\,\phi_\mu\rangle$. These parameters are given in Table 2. The off-diagonal elements of the hamiltonian are calculated according to the modified Wolfsberg–Helmholtz approximation (19). Slater exponents for Ga were increased as compared with the standard parameters (20) in order to fit the calculated band gap with the experimental gap $E_g\approx 4.84$ eV. This is equivalent to give an ionic character to gallium. The orientation axes (*x*, *y*, *z*) for the atomic orbitals, making an orthonormal referential, were chosen such as *x* and *z* are along **a** and **b**, respectively. A 128 *k*-point mesh of the irreducible part of the Brillouin zone was used to compute the density of states curves and crystal orbital overlap populations for the 3D solid. For the individual chains, a 64 *k*-point mesh was used. Dispersion curves were plotted after calculations at $k=0, 0.05, 0.1, \ldots, 0.5$ along each reciprocal axis.

III. BAND STRUCTURE OF GALLIUM OXIDE

The band structure of β-Ga_2O_3 was computed in the energy range −35 to −5 eV and its main features are summed up in Fig. 2 and 3. This energy range includes all the valence bands (Fig. 3) and the conduction bands (Fig. 2) originating from the 4*s* states of gallium. The crystal states originating from the 4*p* gallium states calculated to be above −3 eV are not represented on the graphs. The band folding at $k=0.5$ in Figs. 2a and 2b is a consequence of the screw axis along **b** and the glide plane perpendicular to **b** of the monoclinic $C2/m$ cell. The dispersion curves (Figs. 2a to 2c) and the density of state (DOS) curves (Fig. 2d) clearly show that the conduction states are split into two main groups: the lower one between −9.70 and −8.26 eV and the upper one between −7.56 and −5.32 eV, separated by an indirect 0.70-eV gap along **b***. The projection of the DOS on the 4*s* Ga_I or the 4*s* Ga_{II} AOs (Fig. 2d) is the total DOS weighed by the contribution $c^2_{4s}+\sum_j c_{4s}c_jS_{j,4s}$ of a 4*s* AO to every crystal state in the energy range investigated and averaged over the Brillouin zone. Thus, Fig. 2d reveals two important points: first, the weight of the 4*s* gallium AOs in the conduction bands between −10 and −5 eV is very strong, up to 60%; the second feature is a neat separation between the contributions of octahedral and tetrahedral gallium ions. The 4*s* Ga_{II} AOs belong to the states below −8.26 eV, while the 4*s* Ga_I AOs belong to the states between −7.56 and −5.32 eV. In the valence band, crystal states are separated into two groups (Fig. 3). States between −18 and −14 eV are mainly oxygen 2*p* in composition, while states below −32 eV originate from oxygen 2*s* states. DOS projected on each type of oxygen (sum of the contributions of all AOs centered on a given atom) are represented in Figs. 3a to 3c. These curves show that whatever the energy, oxygen ions contribute equally to the total DOS, though their coordination numbers are different.

In order to explain the origin of the splitting between the 4*s* tetrahedral and the 4*s* octahedral states in the conduction band, we carried out molecular orbital calculations on tetrahedral GaO_4^{5-} and octahedral GaO_6^{9-} clusters with the same geometries as in the solid. The 4*s* level in the tetrahedron (−6.69 eV) lies about 2.24 eV above the 4*s* level in the octahedron (−8.93 eV). If the 3D solid is considered, the cluster levels are broadened into bands by intercell overlaps, which are centered on the original cluster levels. This justifies the higher position of the 4*s* Ga_I bands in the solid and shows that this particular feature of the band structure is a consequence of the local geometries of tetrahedral and octahedral sites. There is thus a discrepancy with the conclusions of Tippins (21). On the basis of a strictly electrostatic model, this author calculated that the octahedral 4*s* gallium states should be higher in energy than the tetrahedral 4*s* gallium states because of the larger coordination number of the octahedral site. In fact, these calculations did not consider the differences in bond lengths between both kinds of clusters. However, Ga–O bonds are significantly shorter in tetrahedral sites (mean distance 1.83 Å) than in octahedral sites (mean distance 2.01 Å). This results in overlap integrals S_{ij} between gallium 4*s* and oxygen 2*s* or 2*p* AOs slightly larger in tetrahedral than in octahedral sites. Typical values for S_{4s-2s} in GaO_4^{5-} and GaO_6^{9-} are 0.14 and 0.10, respectively, and for S_{4s-2p} overlaps values amount to 0.156 in GaO_4^{5-} and to 0.126 only in GaO_6^{-9}. As a consequence, we may expect a higher degree of covalency for Ga_I–O bonds than for Ga_{II}–O bonds in gallium oxide. In this perspective, overlap populations were computed for electron occupation of the crystal orbitals up to E_F and

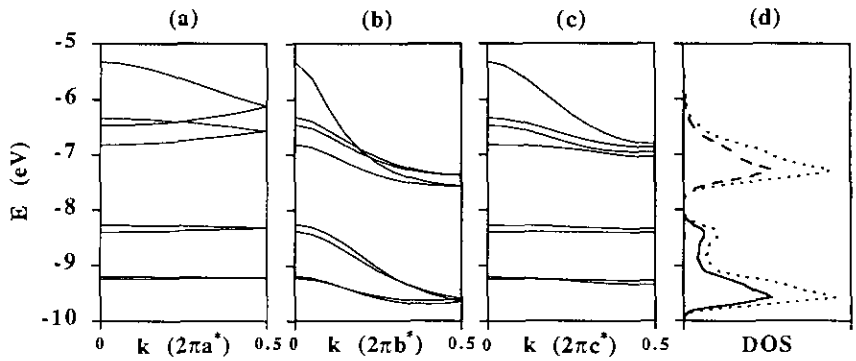

FIG. 2. (a) Dispersion curves in the conduction band of β-Ga_2O_3 along **a***, (b) along **b***, and (c) along **c***. (d) Density of states (DOS) in arbitrary units. Dotted line, total DOS; dashed line, projected DOS on 4s Ga_I AOs; full line, projected DOS on 4s Ga_{II} AOs.

are reported in Table 3 along with bond lengths. Overlap populations are correlated to bond lengths, and the higher the population, the shorter the bond. There is, however, an exception for Ga_I–O_I. Besides, the highest values correspond to the Ga_I–O bonds; this fact is evidence of the higher covalency in tetrahedral sites than in octahedral sites. These conclusions are consistent with Raman spectroscopy (22), which showed that Ga_I–O bonds are stronger, with force constants ranging from 1.62 to 2.25 mdyn · $Å^{-1}$, than Ga_{II}–O bonds, for which force constants range from 0.44 to 1.27 mdyn · $Å^{-1}$. The existence of covalent interactions destabilizes the 4*s* levels into antibonding states, all the more strongly because overlap integrals with the surrounding oxygens are important, and thus explains why the 4*s* octahedral states are lower than the 4*s* tetrahedral states, whether in the clusters or in the solid.

As shown by dispersion curves calculated along **a***, **b***, and **c*** for the 3D solid (Figs. 2a to 2c), the conduction band is strongly anisotropic, with 4*s* Ga_{II} bands much wider along **b*** than along the other reciprocal axes. This indicates that if conduction electrons are present in the conduction band edge, they should be much more delocalized along **b** than perpendicularly to this direction, and thus strongly suggests low-dimensional properties of gallium oxide. In order to confirm this low-dimensional character, we computed the band structure of a tetrahedral single chain and that of an octahedral double chain having the same geometries as in the solid (Figs. 4a and 4b) and compared them to that of the whole solid. For both kinds of chains, the dispersion curves (Figs. 5a and 5b) are very similar in shape and position to the dispersion curves of the 3D solid, calculated along **b*** in the 4*s* Ga_I and the 4*s*

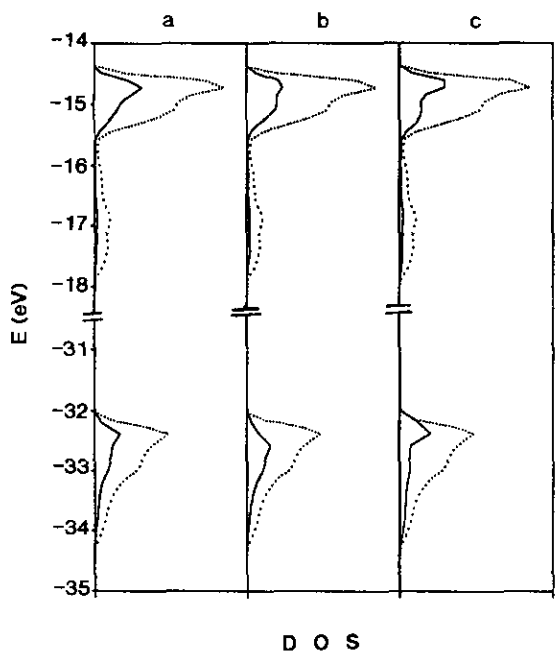

FIG. 3. Density of states (in arbitrary units) in the valence band of β-Ga_2O_3. Dotted line, total DOS; full lines, projected DOS on (a) O_I, (b) O_{II}, and (c) O_{III}. DOS below −32 eV are multiplied by a factor 2.

TABLE 3
Overlap Population Summed up to the Fermi Level and Bond Lengths for the GA–O Bonds in β-Ga_2O_3

Bond	Summed overlap population	Bond length (Å)
Ga_I–O_I	0.26	1.80
Ga_I–O_{II}	0.30	1.83
Ga_I–O_{III}	0.29	1.85
Ga_{II}–O_{II}	0.23	1.95
$Ga_{II}O_I$	0.20	1.98
Ga_{II}–O_{III}[a]	0.17	2.02
Ga_{II}–O_{III}[b]	0.14	2.08

[a] Out of the (**b**, **c**) plane.
[b] In the (**b**, **c**) plane.

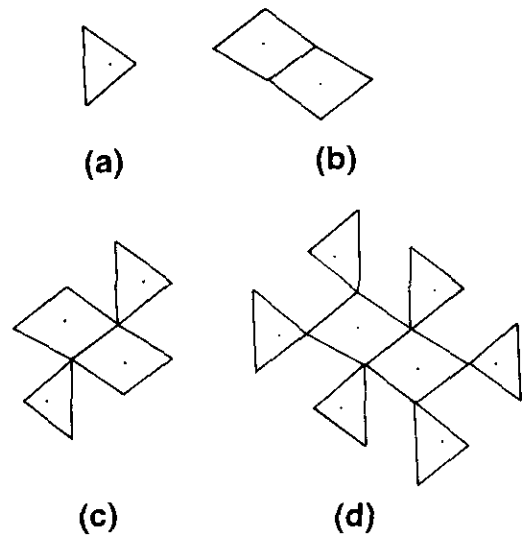

FIG. 4. Structural models for the extended Hückel calculations on chains. (a) Single tetrahedral chain, (b) double octahedral chain, (c) double octahedral chain surrounded by two tetrahedral chains, and (d) double octahedral chain surrounded by six tetrahedral chains. The chain directions (crystallographic vector **b**) are perpendicular to the figure plane.

Ga_{II} bands. The same remark holds for the DOS curves (Figs. 5e and 5f). In particular, the shape of the DOS curve for the isolated octahedral double chain (Fig. 5f) with a maximum at both band edges, which is typical of one-dimensional DOS, is found again for the DOS of the 4*s* Ga_{II} bands of the 3D solid. These strong similarities of dispersion and DOS curves between the 1D isolated chains and the 3D solid indicate that the crystal states making up the conduction bands in β-Ga_2O_3 are practically the electronic states of isolated tetrahedral single chain and octahedral double chain. Figures 5c and 5d show the dispersion curves obtained when the octahedral double chain is surrounded respectively by two and by six tetrahedral chains (Figs. 4c and 4d). As shown by the corresponding DOS curves (Figs. 5g and 5h), states below −8 eV are mainly 4*s* Ga_{II} in composition and those above are 4*s* Ga_I. When the environment of the octahedral double chain is progressively completed by the tetrahedral chains, calculations show only slight alterations of dispersion and DOS curves of each kind of chain. States affected by the interaction between chains are essentially in the vicinity of $k = 0$, in particular, those labeled β, γ', and γ''. The upper tetrahedral levels are shifted upwards, resulting in a tail for the DOS above −6 eV while the upper octahedral levels are lowered below −8 eV, widening the gap between the 4*s* Ga_I and the 4*s* Ga_{II} bands. The fact that these modifications are small shows that the different chains are weakly interacting and thus the energy shifts and the tops of the tetrahedral and octahedral bands respectively may be appropriately described by the usual perturbation formula (23),

$$\Delta e_i \propto \sum_{j \neq i} \frac{S_{ij}^2}{e_i^0 - e_j^0}, \qquad [11]$$

where the e^0's represent the unperturbed energies for isolated tetrahedral and double octahedral chains and S_{ij} are the overlap integrals. A quantitative use of this equation is out of purpose but it emphasizes the fact that the energy shift is all the more pronounced as the interacting states are close in energy. This explains why the upper octahedral state β is much more affected than the lower lying states. This is reflected by the respective weights of 4*s* Ga_I AOs in states α and β. In the β state, coefficients of 4*s* Ga_I are about 0.13–0.20, whereas they are at most of the order of 10^{-2} in α, with values of 0.65 for the coefficients of 4*s* Ga_{II} in both α and β. In other words, electrons in the bottom of the conduction band of gallium oxide are absolutely not affected by the interaction between chains, and they should move as if they were in isolated octahedral double chains and thus should have 1D properties.

These band structure calculations confirm that β-Ga_2O_3 fulfills the conditions mentioned in the Introduction for the existence of the CESR bistability, that is, to know an

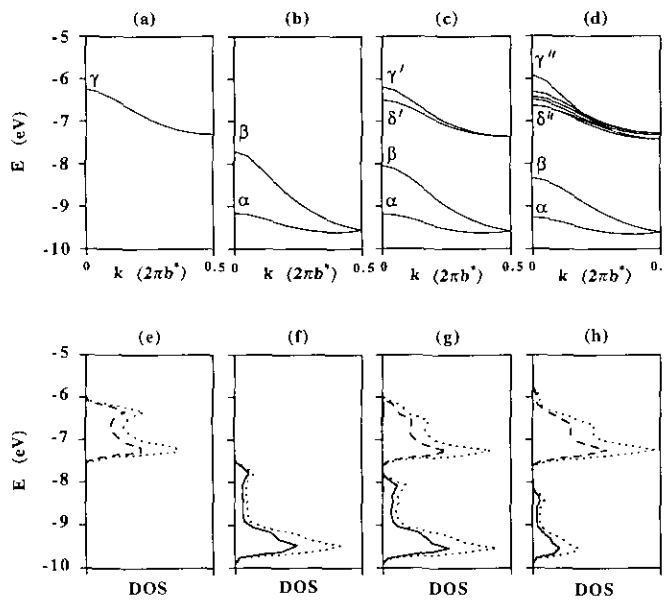

FIG. 5. The four top figures are dispersion curves and the four bottom figures are DOS curves: (a) and (e) correspond to a tetrahedral single chain, (b) and (f) to a double octahedral chain, (c) and (g) to a double octahedral chain linked to two tetrahedral chains, and (d) and (h) to a double octahedral chain linked to six tetrahedral chains. Dotted lines, total DOS; dashed lines, projected DOS on 4s Ga_I AOs; full lines, projected DOS on 4s Ga_{II} AOs.

important contribution (up to 60% of the total DOS) of the 4*s* orbitals in the conduction band, accounting for a strong nuclear polarization, and a pronounced anisotropy of the conduction band that must be at the origin of the narrow EPR linewidth encountered in β-Ga_2O_3. Both points will be discussed in Section V. Moreover, shallow donor states are generally described as a linear combination of the wavefunctions of the bottom of the conduction band; this implies that electrons must have almost the same properties whether they are in donor states or in the conduction band. In particular, this explains why the Overhauser shift and its bistability are observable in the whole temperature range 4–300 K (5).

IV. ESR AND ENDOR OF Ti^{3+} IN β-Ga_2O_3: EVIDENCE OF 1D CATION–CATION INTERACTIONS

General Features

Figures 6a and 7c show two examples of ESR spectra at 110 K of a β-Ga_2O_3 : Ti (0.2%) single crystal. The spectrum is composed of a single broad line with well resolved

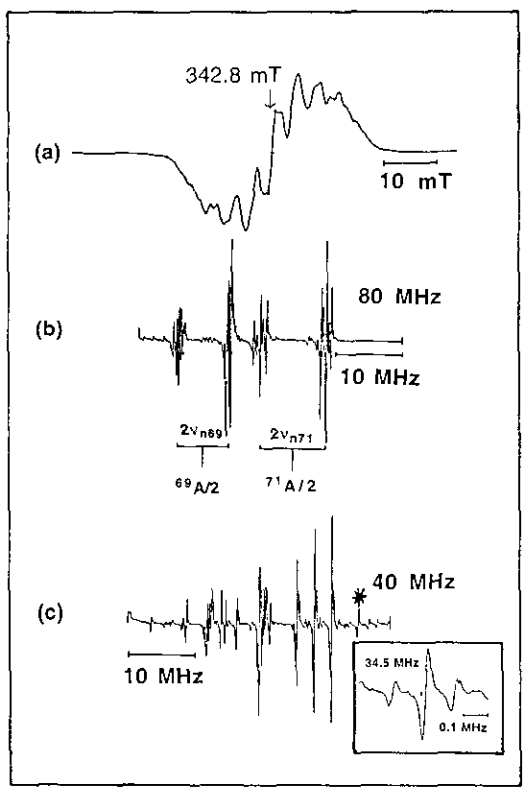

FIG. 6. (a) ESR spectrum of a β-Ga_2O_3 : Ti (0.2%) single crystal with $\mathbf{B}_0$ perpendicular to the (**b**, **c**) plane (*y* direction of the *g*-tensor). (b) and (c) are respectively the high frequency and the low frequency parts of the ENDOR spectrum with $\mathbf{B}_0$ close to the y direction. The inset shows the line marked with an asterisk when $\mathbf{B}_0$ lies in the (**a**, **c**) plane and makes an angle of 20° with **c**.

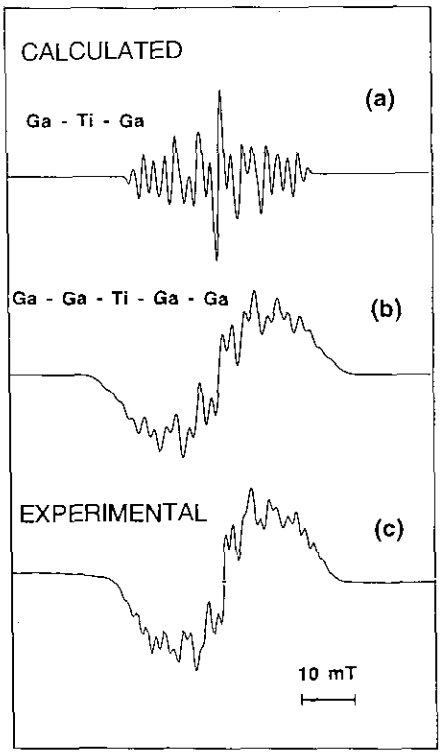

FIG. 7. (a) Calculated ESR spectrum of the linear cluster $[Ga_{II}^{(1)}$–Ti^{3+}–$Ga_{II}^{(1)}]$ with $^{71}A^{(1)} = 5.48$ mT and $\Delta B_{pp} = 1$ mT. (b) Calculated ESR spectrum of the linear cluster $[Ga_{II}^{(2)}$–$Ga_{II}^{(1)}$–Ti^{3+}–$Ga_{II}^{(1)}$–$Ga_{II}^{(2)}]$ with $^{71}A^{(1)} = 5.48$ mT, $^{71}A^{(2)} = 2.22$ mT, and $\Delta B_{pp} = 2.25$ mT. Gaussian lineshapes functions are used in the calculations. (c) Experimental ESR spectrum of a β-Ga_2O_3 : Ti (0.2%) single crystal with $\mathbf{B}_0 \| \mathbf{b}$ (*z* direction of the *g*-tensor).

structure, and characterized by an anisotropic *g*-tensor with principal values $g_z = 1.853$, $g_x = 1.927$, and $g_y = 1.952$. The *z* and *x* axes of the *g*-tensor are parallel to the crystallographic axes **b** and **c**, respectively, and the *y* axis is perpendicular to the (**b**, **c**) plane. These values are typical of Ti^{3+} in an octahedral environment. This is confirmed by UV–visible absorption spectroscopy, showing the existence of a broad band peaking at 510 nm. This absorption corresponds to the $^2T_{2g} \rightarrow {}^2E_g$ absorption of Ti^{3+} in octahedral symmetry and is very similar in shape to the absorption band at 485 nm found for Ti^{3+} in octahedral sites of Al_2O_3 (24). The fact that the *g* axes are parallel to the crystallographic axes and the lack of site splitting of the ESR spectrum show that Ti^{3+} ions occupy octahedral sites without neighboring defects. The hyperfine structure is composed of about 10 to 17 apparent lines when the magnetic field $\mathbf{B}_0$ is parallel to *x* and *y* (Fig. 6a). This structure is more complicated for $\mathbf{B}_0 \| z$, and may contain up to 25 resolved lines (Fig. 7c). A first possible explanation for this splitting is hyperfine interaction with ^{47}Ti ($I = 5/2$, 7.4% natural abundance) and ^{49}Ti ($I = 7/2$, 5.4% natural abundance) nuclei. However this interpretation

must be definitely ruled out because we expect in that case an intense central line flanked by eight weak satellites due to the superposition of ^{47}Ti and ^{49}Ti hyperfine lines. This simple picture contrasts with the multiplicity of lines and the lack of pronounced central line observed in β-Ga_2O_3. The other possible explanation is a superhyperfine (shf) interaction with neighboring gallium nuclei. The existence of two abundant gallium isotopes, ^{69}Ga ($I = 3/2$, $g_n = 1.34439$; 60.1% natural abundance) and ^{71}Ga ($I = 3/2$, $g_n = 1.70818$, 39.9% natural abundance) are likely to be responsible for the complexity of the spectrum and the lack of strong central line since there is no gallium isotope with zero nuclear spin.

A definitive identification of the nuclei responsible for the shf (superhyperfine) structure cannot be obtained from ESR alone since this technique does not give a direct measurement of the nuclear frequency $g_n\beta_nB_0$, which is the only parameter giving unambiguous identification of a nucleus. However, the nuclear frequency can be accurately obtained from ENDOR spectroscopy (16, 25). An ENDOR spectrum is obtained by partial saturation of an ESR line while sweeping the radiofrequency radiation through nuclear resonance transitions. We thus detect NMR transitions of nuclei with nonzero nuclear spin interacting with the unpaired electron spin. In this work we present only preliminary results because ENDOR spectra of β-Ga_2O_3 : Ti^{3+} were found to be very complex and contain more than 140 lines at frequencies ranging from about 0.5 MHz to about 80 MHz. A relative simplification is however obtained for a $\mathbf{B}_0$ orientation close to (but not exactly parallel to) the y axis. Figures 6b and 6c show the high and low frequency parts of the ENDOR spectrum recorded with a magnetic field set at the center of the ESR spectrum (marked with an arrow in Fig. 6a). Let us first consider the high frequency ENDOR spectrum shown in Fig. 6b. For this orientation of $\mathbf{B}_0$, all the ENDOR lines really collapse into four ensembles characterized by the frequencies

$$\nu_{rf} = h^{-1}|m_s A^{(1)} - g_n\beta_nB_0|, \qquad [12]$$

with $m_s = \pm 1/2$ and where A is the shf interaction corresponding to this field orientation. We thus obtain two sets of lines for each gallium isotope. One set at high frequencies is centered about $^{71}A^{(1)}/2$, where $^{71}A^{(1)}$ is the shf interaction with the first neighbor ^{71}Ga nucleus, and split by an amount equal to $2\nu_{n71}$, where $\nu_{n71} = h^{-1}g_{n71}\beta_nB_0$ is the nuclear frequency of ^{71}Ga. The other set of lines is centered about $^{69}A^{(1)}/2$, with $^{71}A^{(1)}/^{69}A^{(1)} = g_{n71}/g_{n69}$, and with a splitting equal to $2\nu_{n69}$. It thus appears evident that Ti^{3+} exhibits a strong shf interaction of about 130 MHz with neighboring gallium nuclei. Upon rotation of $\mathbf{B}_0$ in the (x, y) plane, i.e., for $\mathbf{B}_0 \perp \mathbf{b}$, the different sets of lines are further split by quadrupolar interaction, with $^{71}A^{(1)}$ and $^{69}A^{(1)}$ remaining nearly constant. Upon rotation of $\mathbf{B}_0$ from the (x, y) plane to z, all the ENDOR lines are split and shifted toward high frequencies. This indicates that the shf tensor has a symmetry axis parallel to **b**, showing unambiguously that the gallium nuclei interacting with Ti^{3+} are the first neighbor gallium Ga_{II} located at 3.04 Å along the octahedral chain (**b** axis). The most important part of the low frequency ENDOR spectrum (Fig. 6c) exhibits a complex angular variation, with no revolution symmetry around **b**. This indicates that these lines belong to Ga_I and Ga_{II} neighbors of Ti^{3+} which are placed outside the octahedral double chain running along **b**. There is, however, an exception with the line marked by an asterisk in Fig. 6c. This line has a nearly constant position upon rotation of $\mathbf{B}_0$ around **b**. It also exhibits a quadrupolar splitting, which is maximum for $\mathbf{B}_0 \parallel x$ in the case of the angular variation around **b** (see inset in Fig. 6c). This peculiar angular variation shows that these lines, centered around 34 MHz, belong to the next nearest Ga neighbors if Ti^{3+} along the **b** axis, located at 6.08 Å. If we consider the Ti–Ga distances, these Ga ions correspond in reality to the 20th neighbors. The line marked by an asterisk occurs at a frequency $^{71}A^{(2)} + \nu_{n71}$, where $^{71}A^{(2)}$ is the shf interaction with the 20th neighbor ^{71}Ga nuclei of Ti^{3+} (which is also the second neighbor along **b**). The other lines at $^{71}A^{(2)} - \nu_{n71}$ and $^{69}A^{(2)} \pm \nu_{n69}$ are hidden by the strong lines of the other Ga neighbors and are thus not easily observed. This preliminary ENDOR study essentially shows that Ti^{3+}–Ga shf interactions occurs mainly along **b**, since the interaction with the 20th neighbors, placed along **b**, is larger than the interactions with neighbors 2 to 19. The shf parameters deduced from ENDOR are reported in Table 4. This predominant Ti^{3+}–Ga interaction along **b** justifies the assumption made in the experimental part that Ti^{3+} is in substitutional position since

TABLE 4

Superhyperfine Parameters for Interactions between Ti^{3+} and First (1) and Second (2) Neighbor Gallium Atoms along b in β-Ga_2O_3

	A_x[a]		A_y[a]		A_z[b]		$A_\perp$[c]	
	(MHz)	(mT)	(MHz)	(mT)	(MHz)	(mT)	(MHz)	(mT)
$^{71}Ga^{(1)}$	128.32	4.76	126.8	4.64	142	5.48		
$^{69}Ga^{(1)}$	100.9	3.74	99.7	3.65	109	4.20		
$^{71}Ga^{(2)}$	n.m.		n.m.		n.m.		59.3	2.20
$^{69}Ga^{(2)}$	n.m.		n.m.		n.m.		46.7	1.73

Note. n.m., not measured.

[a] Determined from ENDOR spectra.

[b] Determined from ESR spectrum with $\mathbf{B}_0 \parallel \mathbf{b}$.

[c] Determined from ENDOR spectrum with $\mathbf{B}_0$ in the (**b**, **c**) plane and making an angle of 20° with **c**.

TABLE 5
Configurations of the Three Spectroscopically Different Clusters of Ti with First Neighbor Ga Atoms along b

Cluster	No. of configurations	Probability	No. of ESR transitions
^{69}Ga–Ti–^{69}Ga	1	0.365	7
^{71}Ga–Ti–^{71}Ga	1	0.157	7
^{69}Ga–Ti–^{71}Ga	2	0.478	16

the octahedral interstitial sites in β-Ga_2O_3 have no gallium neighbor along **b**.

Simulation of the ESR Spectrum

Despite the preliminary character of this ENDOR study, it shows that the Ti^{3+}–Ga interactions along **b** largely exceed interactions perpendicular to **b**. One can thus consider Ti^{3+} in β-Ga_2O_3 as a [$Ga_{II}^{(2)}$–$Ga_{II}^{(1)}$–Ti^{3+}–$Ga_{II}^{(1)}$–$Ga_{II}^{(2)}$] cluster oriented along **b**. Here $Ga_{II}^{(1)}$ and $Ga_{II}^{(2)}$ indicate respectively the first and second neighbor of Ti^{3+} along an octahedral chain. Recalling that gallium possesses two different isotopes, we thus expect 16 different configurations for this cluster, which implies an ESR spectrum containing 900 different transitions as will be shown below, determined by only the two shf parameters, $^{71}A^{(1)}$ and $^{71}A^{(2)}$, the shf interactions with the first and the second neighbor ^{71}Ga nuclei along **b**, respectively. The corresponding interactions for ^{69}Ga nuclei are obtained from the relation $^{71}A^{(i)}/^{69}A^{(i)} = 1.2706$, the ratio of the g_n factors. The simulation of the ESR spectrum thus provides a severe test for this defect model. Since the best ESR resolution was achieved for $\mathbf{B}_0 \parallel \mathbf{b}$ (Fig. 7c), this field orientation was chosen for the simulation. The latter was performed in two steps. In the first one, we calculated the ESR spectrum by taking into account only the first neighbor gallium nuclei, which corresponds to the case of a linear cluster [$Ga_{II}^{(1)}$–Ti^{3+}–$Ga_{II}^{(1)}$]. Three different isotope configurations (Table 5) contribute to the total spectrum, which give a resulting ensemble of 30 transitions as shown by the stick diagram represented in Fig. 8. The theoretical spectrum of Fig. 8 is governed by only one parameter which is the shf interaction $A_z^{(1)}$ with one of the two gallium isotopes in first neighbor position $^{71}A_z^{(1)} = 5.48$ mT. Figure 7a shows the spectrum calculated from the stick diagram of Fig. 8 by using a gaussian lineshape function with peak to peak linewidth $\Delta B = 1$ mT. Although the overall width of the total spectrum is close to the experimental one, shown in Fig. 7c, and the major lines of the shf structure are present, it is clear that there is a net discrepancy between calculated and experimental spectra. In particular, the calculated spectrum contains only 17 lines instead of 25 in the experimental one, and the broad component of the experimental spectrum is not obtained in the calculated one. Taking a larger linewidth provokes a collapse and a reduction of the number of lines without introducing any wide background line, while a smaller linewidth only splits the shf lines into their components without providing any better agreement with the experimental spectrum.

If we now take into account the next nearest neighbors along **b**, the species considered is a linear cluster [$Ga_{II}^{(2)}$–$Ga_{II}^{(1)}$–Ti^{3+}–$Ga_{II}^{(1)}$–$Ga_{II}^{(2)}$], which possesses 16 different isotopic configurations, with a total number of transitions which amounts to 900 (Table 6). Figure 9 shows the corresponding stick diagram, calculated with the shf parameters $^{71}A_z^{(1)} = 5.48$ mT and $^{71}A_z^{(2)} = 2.22$ mT. Because of the great number of lines, it was impossible to label the nuclear quantum number of the transitions, as is the case with the cluster [$Ga_{II}^{(1)}$–Ti^{3+}–$Ga_{II}^{(1)}$] (Fig. 8). The total spectrum shown in Fig. 7b was calculated from the stick diagram of Fig. 9 by using gaussian lineshape functions with peak to peak linewidth $\Delta B = 2.25$ mT. Despite the fact that the agreement between experimental and calculated spectra is not perfect, some important improvements have been made as compared with the previous one. Six lateral supplementary lines have appeared as well as a wide background line, and the relative intensities of the shf lines are in better agreement than in the first simulation. Moreover, it is noteworthy that the gross features of the spectrum are contained in a spectrum of 900 transitions calculated with only one adjustable parameter, the linewidth (ΔB). The small discrepancies could be due to contributions from gallium nuclei located outside the linear cluster [$Ga_{II}^{(2)}$–$Ga_{II}^{(1)}$–Ti^{3+}–$Ga_{II}^{(1)}$–$Ga_{II}^{(2)}$]. Such interactions are in fact expected from the low frequency ENDOR spectra (Fig. 6c).

Interpretation of the Superhyperfine Parameters

The knowledge of the shf coupling constants can provide important information on the orbital composition of the ground state of Ti^{3+} in β-Ga_2O_3, in particular, on the degree of admixture of the Ti $3d$ orbitals with the $4s$ orbitals of the neighbor gallium ions along **b**. In the most general way, the wave function $|\Psi_0\rangle$ of the ground state of Ti^{3+} can be expanded as follows:

$$|\Psi_0\rangle = a|\Psi_{3d}\rangle + 2b^{(1)}|\Psi_{4s}^{(1)}\rangle + 2b^{(2)}|\Psi_{4s}^{(2)}\rangle + \sum_{i=3}^{N} 2b^{(i)}|\Psi_{4s}^{(i)}\rangle + c|\Psi\rangle. \quad [13]$$

Here $|\Psi_{3d}\rangle$ is a linear combination of the $3d$ AOs of Ti appropriate to the site symmetry C_s, $|\Psi_{4s}^{(i)}\rangle$ are the $4s$ AOs of the ith neighbors along **b**, and $|\psi\rangle$ is a linear combination of other AOs interacting with Ti^{3+}. It is of great interest to calculate the $b^{(i)}$'s for it gives an idea of the extension

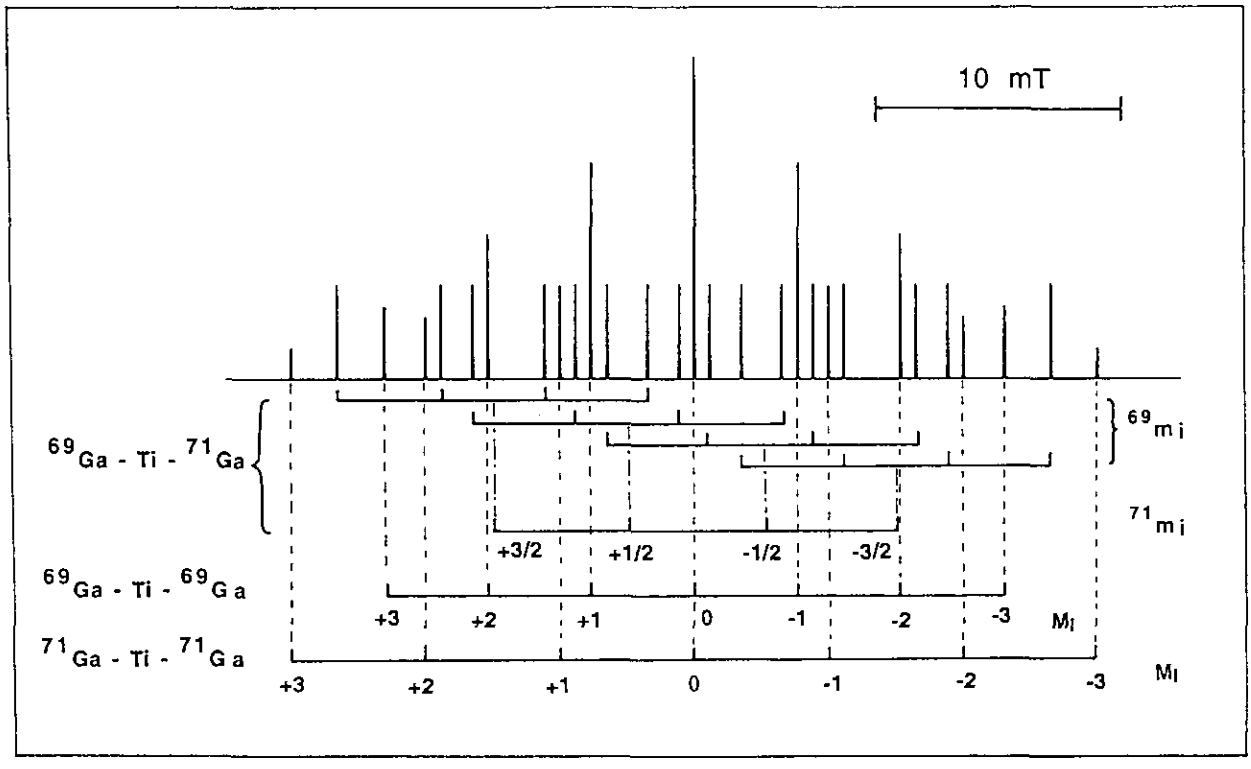

FIG. 8. Stick diagram showing the ESR transitions of the linear cluster $[Ga_{II}^{(1)}-Ti^{3+}-Ga_{II}^{(1)}]$. $^{69}m_i$ and $^{71}m_i$ correspond respectively to the nuclear spin quantum numbers of ^{69}Ga and ^{71}Ga. For the sake of clarity, the values of $^{69}m_i$ are not indicated; they range from +3/2 to −3/2 by step of 1 from the left end to the right end of each rake. M_I labels correspond to the sum of the nuclear spin quantum numbers of both neighbors for the one-isotope clusters.

of the ground state wave function of Ti^{3+} along **b**. If the electron in the ground state of Ti^{3+} is partially delocalized in the 4*s* AOs of the neighboring gallium ions, it creates an electron spin density ρ_{Ga} at their nuclei, which is responsible for a Fermi contact interaction:

$$^{69/71}A_{iso}^{(i)} = \frac{8\pi}{3h} g\beta g_{n69/71}\beta_n \rho_{Ga}^{(i)}. \quad [14]$$

This interaction gives the isotropic contribution to the shf tensor corresponding to the *i*th neighbor along **b**. The spin density $\rho_{Ga}^{(i)}$ is linked to the coefficient $b^{(i)}$ by

$$\rho_{Ga}^{(i)} = |b^{(i)}|^2 |\Psi_{4s}(0)|^2. \quad [15]$$

$\Psi_{4s}(0)$ is the amplitude of the 4*s* AO of a gallium at its nucleus. Thus $^{69/71}A_{iso}^{(i)}$ can be written as

$$^{69/71}A_{iso}^{(i)} = |b^{(i)}|^2\, ^{69/71}A_{iso}, \quad [16]$$

where $^{69/71}A_{iso}$ corresponds to the scalar hyperfine interaction of an isolated Ga^{2+} ion (configuration $4s^1$). This value can be estimated from that measured for $^{71}Ga^{2+}$ in ZnS (26), which is equal to $^{71}A_{iso} \approx 7800$ MHz. Then, if the value of $^{71}A_{iso}^{(i)}$ is known, $|b^{(i)}|$ can be obtained from Eq. (16). The value $^{71}A_{iso}^{(i)}$ is normally determined from the principal values of the shf tensor by $^{71}A_{iso}^{(i)} = (1/3)(^{71}A_x^{(i)} + {}^{71}A_y^{(i)} + {}^{71}A_z^{(i)})$. The latter could be determined for the first neighbors along **b**: $^{71}A_{iso}^{(1)} \approx 138$ MHz. For the second neighbors, only one value of the shf tensor

TABLE 6
Configurations of the Possible Linear Ga–Ga–Ti–Ga–Ga Clusters

Cluster	No. of configurations	Probability	No. of ESR transitions
^{69}Ga–^{69}Ga–Ti–^{71}Ga–^{71}Ga	4	0.229	256
^{69}Ga–^{69}Ga–Ti–^{71}Ga–^{69}Ga	2	0.1745	112
^{69}Ga–^{69}Ga–Ti–^{69}Ga–^{71}Ga	2	0.1745	112
^{69}Ga–^{69}Ga–Ti–^{69}Ga–^{69}Ga	1	0.133	49
^{69}Ga–^{71}Ga–Ti–^{71}Ga–^{71}Ga	2	0.075	112
^{71}Ga–^{69}Ga–Ti–^{71}Ga–^{71}Ga	2	0.075	112
^{69}Ga–^{71}Ga–Ti–^{71}Ga–^{69}Ga	1	0.057	49
^{71}Ga–^{69}Ga–Ti–^{69}Ga–^{71}Ga	1	0.057	49
^{71}Ga–^{71}Ga–Ti–^{71}Ga–^{71}Ga	1	0.025	49

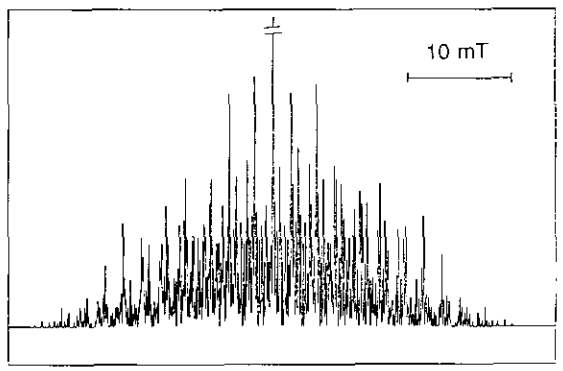

FIG. 9. Stick diagram showing the 900 theoretical ESR transitions of the linear cluster $[Ga_{II}^{(2)}-Ga_{II}^{(1)}-Ti^{3+}-Ga_{II}^{(1)}-Ga_{II}^{(2)}]$.

could be measured (see Table 4), along a direction perpendicular to **b**: $^{71}A_{\perp}^{(2)} \approx 59.3$ MHz. However, the anisotropic part of the shf tensor did not exceed 3% of the total value in the case of the first neighbors, and it should be much lower for the second neighbors. Therefore we can reasonably take: $^{71}A_{iso}^{(2)} \approx {}^{71}A_{\perp}^{(2)} \approx 59.3$ MHz. Hence, from $^{71}A_{iso}^{(1)}$ and $^{71}A_{iso}^{(2)}$, we obtain the values of the coefficient of the 4*s* AOs of the first and second neighbor gallium ions along **b** in the ground state of Ti^{3+}: $|b^{(1)}| \approx 0.13$ and $|b^{(2)}| \approx 0.09$. Both values are not very different, showing that the ground state wave function of Ti^{3+} decreases slowly along *b*. Therefore we can expect non negligible interactions between Ti^{3+} and gallium ions located farther than the second neighbor position along **b**. Such interactions must also contribute to the low frequency part of the ENDOR spectra. A second point is that these coefficients reveal an important admixture with the neighboring 4*s* AOs, thus indicating that the ground state of Ti^{3+} is relatively close in energy to the bottom of the conduction band.

In conclusion, the ground state of Ti^{3+} interacting with the neighboring gallium ions can be represented as a bonding combination of the Ti states in the forbidden band gap and the crystal states of the conduction band edge. With this point in mind, several remarks can be driven from the ESR-ENDOR investigation of Ti^{3+} in octahedral sites of β-Ga_2O_3, confirming the major conclusions of the band structure calculations:

(i) The fact that the shf tensor is essentially isotropic and that the presence probability of the electron of Ti^{3+} on the first and second neighboring gallium ions along **b** is not negligible agrees with the predominant 4*s* gallium character of the conduction band.

(ii) The predominant 1D cation–cation interactions along **b** and the large extension of the Ti^{3+} ground state along this axis confirms the one dimensionality of the conduction band.

(iii) Only interactions between Ti^{3+} and octahedral gallium ions are evidenced. This shows that the 4*s* octahedral gallium states are lower in energy than the 4*s* tetrahedral states, as foreseen by the band structure calculations.

V. RELATION BETWEEN ELECTRON BAND STRUCTURE AND MAGNETIC BISTABILITY OF CONDUCTION ELECTRONS IN β-Ga_2O_3

We shall now return to the most striking property of β-Ga_2O_3, which is the magnetic bistability of the conduction electrons. The resonance condition of the conduction electron spins is given by

$$h\nu = g\beta(B_0 + B_n), \qquad [17]$$

where the effective field seen by the electron spins $B_{eff} = B_0 + B_n$ is composed of the external field B_0 and the internal nuclear field B_n created by the nuclear polarization of nuclear spins. A significant value of B_n is obtained upon saturation of the CESR signal, the so-called Overhauser effect (4). We have previously shown that B_n is sufficiently strong in β-Ga_2O_3 to exhibit a bistability, i.e., two stable values of B_n can exist for the same values of the external parameters T, ν, B_0, and P (the incident microwave power) (3, 5). The first condition to obtain a dynamic nuclear polarization by the Overhauser effect is that the electron spins interact with each nuclear spin by a Fermi contact interaction given by

$$A = \frac{8\pi}{3h} g\beta g_n \beta_n \rho_{Ga}, \qquad [18]$$

where ρ_{Ga} is the electron spin density at the Ga nucleus. If the electron spins interact with N equivalent nuclei, the resulting nuclear field B_n created by saturation of the electron spin resonance is given by the expression (5, 8)

$$B_n = \frac{I(I+1)NAf}{3kT} B_0 s, \qquad [19]$$

with $I = 3/2$ for Ga nuclei, and where s is the saturation factor of the resonance, which can vary between 0 for thermal equilibrium and 1 for complete saturation. The parameter f is the "leakage factor," which, in other words, represents the efficiency of the nuclear polarization via hyperfine interaction. The maximum value $f = 1$ is obtained if the nuclear relaxation is solely due to a flip-flop mechanism $\Delta(m_s + m_I) = 0$ where a nuclear spin "flops" when an electron spin "flips." If nuclear relaxation occurs also by other mechanisms, the leakage factor is given by (2)

$$f = \frac{1/T_x}{1/T_x + \sum_i 1/T_{ni}}, \qquad [20]$$

where T_x is the "flip-flop" relaxation time and the T_{ni}'s represent the relaxation times due to other mechanisms. The highest theoretical value of B_n is obtained for $f = 1$ and $s = 1$ and the NA value as high as possible. For an electron delocalized over an ensemble of $^{71}Ga^{3+}$ ions, the hyperfine interaction is only due to the scalar interaction given by Eq. (18), where ρ_{Ga} is equal to $|\Psi_{4s}(0)|^2/N$, with $\Psi_{4s}(0)$ being the amplitude of the $4s$ wavefunction of gallium at the nucleus. If the nuclear relaxation occurs only by a flip-flop mechanism, one obtains $f = 1$ (which is reasonable since $1/T_x$ is proportional to A^2 (2)). In this simple ideal case, NAf in Eq. (19) is equal to

$$NAf = {}^{71}A_{iso} \approx 7800\ \text{MHz}. \quad [21]$$

This value corresponds to the scalar hyperfine interaction $^{71}A_{iso}$ of an isolated $^{71}Ga^{2+}$ ion (26). For the actual interaction corresponding to β-Ga_2O_3, where the unpaired electrons are delocalized in a conduction band and are in contact with both ^{71}Ga and ^{69}Ga nuclei, NAf in Eq. (19) should be replaced by a mean value $\langle NAf\rangle$ given by the following expression (5):

$$\langle NAf\rangle = 6800 \cdot f \cdot \sum_{i=1}^{N} |a_i|^2 \quad \text{(MHz)}. \quad [22]$$

The numerical factor 6800 MHz is the hyperfine interaction of a $4s$ electron in isolated Ga^{2+} (configuration $(4s)^1$); it is an average value for both gallium isotopes ^{69}Ga and ^{71}Ga. In this equation an average factor f is also considered. The parameter a_i is the coefficient of the $4s$ AO of the ith gallium in the crystal orbital at the bottom of the conduction band. The sum in Eq. (22) can be restricted to a sum over the eight gallium ions in one single cell because of the translational symmetry:

$$\langle NAf\rangle = 6800 \cdot f \cdot \sum_{i=1}^{8} |c_i|^2. \quad [23]$$

Here the c_i's are the actual coefficients given by the calculation program and are normalized over one cell. Calculations over several k-points in the Brillouin zone indicates that the bottom of the conduction band is close to $\mathbf{k} = (0, 0.4, 0)$. In any case, the quasi-constant proportion of $4s$ AOs in the total DOS of the conduction band shown in Fig. 2d allows us to assume reasonably that $\sum_{i=1}^{8} |c_i|^2$ does not vary significantly with $\mathbf{k}$. Using the c_i coefficients at $\mathbf{k} = (0, 0.4, 0)$, we found

$$\sum_{i=1}^{8} |c_i|^2 \approx 0.84, \quad [24]$$

which gives

$$\langle NAf\rangle \approx 5712 \cdot f \quad \text{(MHz)}. \quad [25]$$

Up to now, no experimental value of f has been determined, so that Eq. (25) can only be used to give an estimation of f. With an experimental value $\langle NAf\rangle \approx 3020$ MHz at room temperature (5), we finally get $f \approx 0.5$. For the moment, the sole indication of validity of this calculation is that the calculated f value lies in the expected range 0 to 1. Anyhow, since f depends on the nuclear relaxation times, it must be very sensitive to crystal defects and impurities that could influence the relaxation times. We actually noted variations in the intensity of the Overhauser shift and in the width of hysteresis among our samples that could be related to impurity contents. Therefore, if the calculated value $f = 0.5$ is correct, the bistable Overhauser effect in gallium oxide could be in principle greatly enhanced by improving the elaboration method in order to achieve a value of f as close as possible to 1.

Along with a strong Overhauser shift, the second condition to observe a CESR bistability is a small ESR linewidth. We shall see now that the significant anisotropy of the band structure of β-Ga_2O_3 can be responsible for the very narrow ESR line (about 0.05 mT) encountered in this compound. The unsaturated ESR linewidth ΔB_{pp} is determined by the transverse relaxation time T_2 of the electron spins via

$$\Delta B_{pp} = \frac{2}{\gamma_e \sqrt{3} T_2}. \quad [26]$$

In the general case the relaxation rate is the sum of a spin–spin dipolar contribution $1/T_2^{s-s}$ and spin–phonon contribution $1/T_2^{s-p}$:

$$1/T_2 = 1/T_2^{s-s} + 1/T_2^{s-p}. \quad [27]$$

In β-Ga_2O_3, spins are diluted ($<10^{19}$ cm^{-3}) and the ESR linewidth is motionally narrowed so that the spin–spin component in Eq. (27) vanishes. Therefore the ESR linewidth is exclusively determined by the spin–phonon relaxation, which in conductors usually occurs via Elliott's mechanism (27):

$$1/T_2^{s-p} \approx a \frac{(\Delta g)^2}{\tau_r}. \quad [28]$$

In this expression, which normally holds for an isotropic conductor, Δg is the g shift from the free electron value $g_e = 2.0023$, τ_r is the relaxation time characteristic of the conductivity, and a is a constant of the order of unity. A straightforward application of Eq. (28) requires the knowledge of τ_r. An estimation of its value can be obtained from the electron mobility at room temperature measured

by Lorentz *et al.* (1) $\mu \approx 80\ \mathrm{cm^2\ V^{-1}\ s^{-1}}$ and the effective mass estimated by Aubay (28) $m^* \approx 0.3\ m_e$. From the expression of τ_r,

$$\tau_r = \frac{\mu m^*}{e}, \qquad [29]$$

we get $\tau_r \approx 1.4 \times 10^{-14}$ s. In β-Ga_2O_3, the components of the g-tensor are $g_x = 1.9590$, $g_y = 1.9616$, and $g_z = 1.9635$, thus giving a mean g shift $\langle \Delta g \rangle \approx 0.041$. Using the values of τ_r and $\langle \Delta g \rangle$ in Eq. (28), we get

$$T_2^{s-p} \approx 9 \times 10^{-12}\ \mathrm{s}. \qquad [30]$$

This value is almost five orders of magnitude lower than the value deduced experimentally from linewidth measurement $T_2 \approx 2.5 \times 10^{-7}$ s at room temperature. This discrepancy between the experimental value of T_2 and that calculated from Elliott's theory should be related to the particularly low-dimensional character of the band structure of β-Ga_2O_3. As a matter of fact, the narrowest ESR linewidths are met in one-dimensional organic conductors, constituted by the stacking of structural units along one direction. Several works on such low-dimensional conductors (9) showed that Eq. (28) can be adapted in order to take into account the anisotropy of the band structure by introducing the ratio of the transfer integrals $t_\perp$ and $t_\parallel$ respectively perpendicular and parallel to the chain direction of the structure so that

$$1/T_2^{s-p} \approx a \frac{|t_\perp|^2}{|t_\parallel|^2} \frac{(\Delta g)^2}{\tau_r}. \qquad [31]$$

This expression emphasizes the fact that in case of low-dimensional electronic structure, which corresponds to $|t_\perp|^2/|t_\parallel|^2 \ll 1$, the ESR linewidth can be strongly reduced as compared with a 3D conductor, all other parameters kept constant. In the case of β-Ga_2O_3, we have seen in Section III that the conduction electrons essentially moved along the double octahedral chains, so that the longitudinal integral $t_\parallel$ corresponds to the motion along these chains and the perpendicular integral corresponds to the tunneling from one double chain to another through the barrier potential created by the tetrahedral chains in between. If we assume that transfer integrals are roughly proportional to bandwidths, a reasonable estimate of $|t_\perp|^2/|t_\parallel|^2$ can be provided by the calculation of the band structure of a two-dimensional structural model made of an octahedral double chain repeated periodically perpendicularly to the chain direction. With this model, the bandwidths along reciprocal directions respectively parallel and perpendicular to the chain axis are calculated to be $\Delta E_\parallel \approx 0.445$ eV and $\Delta E_\perp \approx 10^{-3}$ eV. With $|t_\perp|^2/|t_\parallel|^2 \approx |\Delta E_\perp|^2/|\Delta E_\parallel|^2 \approx 5 \times 10^{-6}$ and $a \approx 1$, Eq. (31) gives

$$T_2 \approx 1.8 \times 10^{-6}\ \mathrm{s}. \qquad [32]$$

Though this value is not exactly equal to the measured one, the agreement is now better than in the case of the value calculated on the basis of an isotropic model. The fact that the introduction of the anisotropy of the band structure via the factor $|t_\perp|^2/|t_\parallel|^2$, allows to gain several orders of magnitude in the calculated T_2 and to near the actual value shows that low dimensionality can actually explain the narrow ESR line in gallium oxide. However, the relation between dimensionality and ESR linewidth (and thus bistability) remains to be studied thoroughly. In this prospect, a deeper understanding of the ESR relaxation mechanism in β-Ga_2O_3 in connection with the dynamic properties of the conduction electrons needs to be achieved.

VI. CONCLUSION

We have studied in this paper the band structure of gallium oxide by the crystalline extension of the extended Hückel method. The principal features are the following:

(i) The conduction band has a strong 4*s* character ($\approx 60\%$).

(ii) The 4*s* contribution to the lowest conduction bands is provided exclusively by the octahedral gallium ions.

(iii) The band structure is strongly anisotropic with bands much larger along **b*** than along **a*** or **c***.

The 1D character of the conduction band and its predominantly 4*s* Ga_{II} character was confirmed by ESR and ENDOR study of the paramagnetic probe Ti^{3+}, located in the Ga_{II} site, which shows the existence of a strong Ti(3*d*)–Ga(4*s*) overlap up to the second neighbor along the **b** direction.

The characteristics of the conduction band were also found to be directly responsible for the bistable hysteresis of the conduction electron spin resonance (BCESR phenomenon):

(i) The predominant 4*s* gallium character of the conduction band is directly responsible for the intense nuclear field B_n created by the Overhauser effect. The estimated value $f \approx 0.5$ of the leakage factor suggests that B_n could be larger if the other sources of nuclear relaxations, for example, relaxation by magnetic impurities, can be suppressed.

(ii) The pronounced 1D character of the conduction band appears likely to be responsible for the very small value of the CESR linewidth, which was found to be a prerequisite for the existence of the BCESR phenomenon.

This confirms our previous expectation that the ideal

model compound for the obtention of a strong BCESR would be a 1D organometallic conductor whose conduction band is essentially made of s orbitals of elements such as Ga, In, Tl, Cs, Cu, ... (7).

This work also offers new perspectives concerning β-Ga_2O_3. For sufficiently reduced samples, the concentration of shallow donors is high enough to give a donor band, responsible for a nearly constant conductivity from 4 K to room temperature (5). Moreover, the strong anisotropy of the conduction band suggests that the conductivity should be also anisotropic, with a quasi-metallic behavior along **b**. However, detailed conductivity and Hall measurements along the different cristallographic axes are still lacking. Such techniques, associated with time-resolved ESR spectroscopy, could provide a deeper insight into the original electronic and magnetic properties of gallium oxide.

ACKNOWLEDGMENTS

The authors gratefully acknowledge Mr. G. Dhalenne from the Laboratoire des Composés Non-Stoechiométriques (URA 446 CNRS) for the synthesis of one of the β-Ga_2O_3 : Ti crystals by the floating zone method. They are also indebted to Mrs. A. M. Lejus for her contribution to the synthesis of β-Ga_2O_3 : Ti crystals by the Verneuil method.

REFERENCES

1. M. R. Lorenz, J. F. Woods, and R. J. Gambino, *J. Phys. Chem. Solids,* **28,** 403 (1967).
2. A. Abragam, "Principles of Nuclear Magnetism," Clarendon Press, Oxford, 1986.
3. E. Aubay and D. Gourier, *J. Phys. Chem.* **96,** 5513 (1992).
4. A. Overhauser, *Phys. Rev.* **92,** 411 (1953).
5. E. Aubay and D. Gourier, *Phys. Rev. B* **47,** 15023 (1993).
6. G. Sachs, W. Stöcklein, B. Bail, E. Dormann, and M. Schwoerer, *Chem. Phys. Lett.* **89,** 179 (1982).
7. E. Aubay and D. Gourier, *Solid State Commun.* **85,** 821 (1993).
8. M. Gueron and C. Ryter, *Phys. Rev. Lett.* **3,** 338 (1959).
9. (a) Y. Tomkiewicz and A. R. Taranko, *Phys. Rev. B* **18,** 733 (1978); (b) T. Takahashi, H. Doi, and H. Nagasawa, *J. Phys. Soc. Jpn.* **48,** 423 (1980).
10. Ph. Turek, J. J. André, and J. Simon, *Solid State Commun.* **63,** 741 (1987).
11. S. Geller, *J. Chem. Phys.* **33,** 676 (1960).
12. M. H. Whangbo and R. Hoffmann, *J. Am. Chem. Soc.* **100,** 6093 (1978).
13. (a) T. Harwig, F. Kellendonk, and S. Slappendel, *J. Phys. Chem. Solids* **39,** 675 (1978); (b) T. Harwig and F. Kellendonk, *J. Solid State Chem.* **24,** 255 (1978); (c) T. Harwig, G. J. Wubbs, and G. J. Dirksen, *Solid State Commun.* **18,** 1223 (1976); (d) T. Harwig and J. Schoonman, *J. Solid State Chem.* **23,** 205 (1978); (e) F. Eba and P. Gode, *C. R. Acad. Sci. Paris* **29,** C61 (1980); (f) J. Rasneur, F. Eba, P. Lafollet, and J. P. Delmaire, *Rev. Int Hautes Temp. Refract. Fr.* **27,** 91 (1991); (g) L. N. Cojocaru and I. D. Alecu, *Z. Phys. Chem. N. F.* **84,** 325 (1973); (h) L. N. Cojocaru, *Rev. Roum. Phys.* **18,** 409 (1973); (i) L. N. Cojocaru and A. Prodan, *Rev. Roum. Phys.* **19,** 209 (1974); (j) T. Sasaki and K. Hijikata, *Proc. Inst. Nat. Sci. Nihon Univ.* **9,** 29 (1974); (k) F. BozonVerduraz, C. Poitevin, and G. Pannetier, *J. Chim. Phys. (France)* **67,** 1608 (1970); (l) F. Bozon-Verduraz and C. Poitevin, *J. Chim. Phys. (France)* **73,** 43 (1976).
14. See, for example, J. Sigg, Th. Prisner, K. P. Dinse, H. Brunner, D. Schweitzer, and K. H. Hauser, *Phys. Rev. B* **27,** 5366 (1983); G. G. Maresh, A. Grupp, M. Mehring, J. U. v. Schütz, and H. C. Wolf, *J. Phys. (France)* **46,** 461 (1985).
15. D. R. Taylor, J. Owen, and B. M. Wanklyn, *J. Phys. C* **6,** 2592 (1973).
16. J. M. Spaeth, J. R. Niklas and R. H. Bartram, "Structural Analysis of Point Defects in Solids." Springer Series in Solid State Science, Vol. 43. Springer, Berlin, 1992.
17. M. Saurat, A. Revcolevski, and R. Collongues, *C. R. Acad. Sci. Paris* **271c,** 58 (1970).
18. A. B. Chase, *J. Am. Ceram. Soc.* **47,** 470 (1964).
19. J. H. Ammeter, H.-B. Bürgi, J. C. Thibeault, and R. Hoffmann, *J. Am. Chem. Soc.* **100,** 3686 (1978).
20. C. Minot and C. Demangeat, *J. Chim. Phys. (France)* **87,** 931 (1990).
21. H. H. Tippins, *Phys. Rev.* **140,** A316 (1965).
22. D. Dohy and J. R. Gavarri, *J. Solid State Chem.* **49,** 107 (1983).
23. T. A. Albright, J. K. Burdett and M. H. Whangbo, "Orbital Interactions in Chemistry," p. 32. Wiley–Interscience, New York, 1985.
24. P. F. Molton, *J. Opt. Soc. Am. B* **3,** 125 (1986).
25. G. Feher, *Phys. Rev.* **103,** 834 (1956).
26. A. Raüber and J. Schneider, *Phys. Status Solidi* **18,** 125 (1966).
27. R. J. Elliott, *Phys. Rev.* **96,** 266 (1954).
28. E. Aubay, Ph.D. thesis, Paris, 1992.